Resource

Chemistry & Biology

# A Mass Spectrometry Platform for a Streamlined Investigation of Proteasome Integrity, Posttranslational Modifications, and Inhibitor Binding

## Graphical Abstract

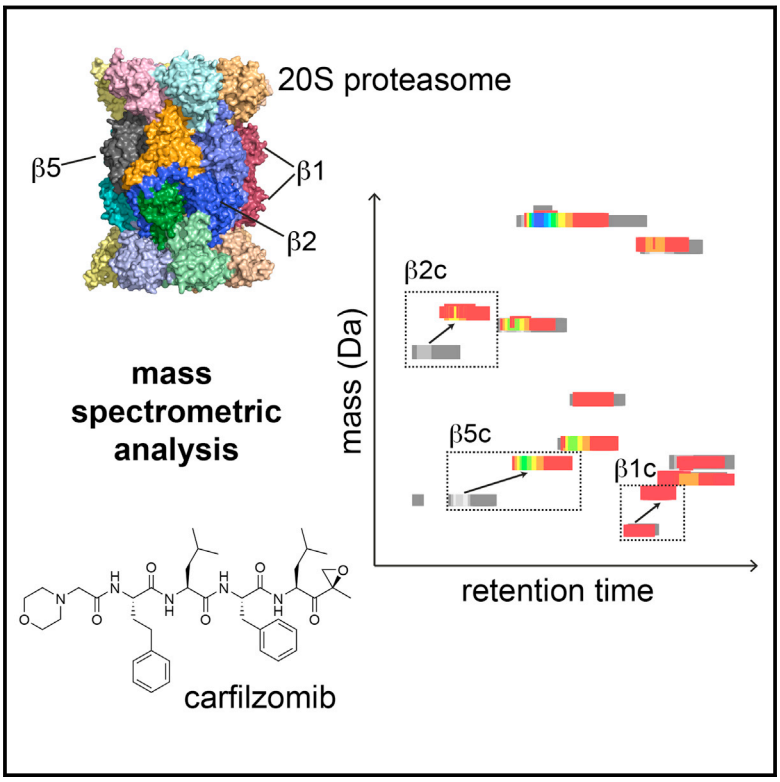


## Authors

Malte Gersch, Mathias W. Hackl, ..., Michael Groll, Stephan A. Sieber

## Correspondence

stephan.sieber@mytum.de

## In Brief

Intact protein mass spectrometry allows determination of properties of protein complexes that are difficult to obtain through peptide-based methods. Gersch et al. introduce an analytical platform for the streamlined analysis of proteasome samples, revealing phosphorylation stoichiometries, inhibitor specificity, and sample heterogeneities.

## Highlights

- Intact protein mass spectrometry reveals proteasome sample heterogeneity
- Quantitative phosphorylation stoichiometries of α7 subunits are obtained
- Sample maps visualize subunit preferences of covalent proteasome inhibitors
- A software tool for rolling-window spectral deconvolution is introduced

Gersch et al., 2015, Chemistry & Biology 22, 404–411
March 19, 2015 
http://dx.doi.org/10.1016/j.chembiol.2015.01.004

CellPress

CellPress

Chemistry & Biology
Resource

# A Mass Spectrometry Platform for a Streamlined Investigation of Proteasome Integrity, Posttranslational Modifications, and Inhibitor Binding

Malte Gersch,[1] Mathias W. Hackl,[1] Christian Dubiella,[1] Alexander Dobrinevski,[1] Michael Groll,[1] and Stephan A. Sieber[1,*]
[1]Department of Chemistry and Center for Integrated Protein Science Munich (CIPS[M]), Technische Universität München, Lichtenbergstraße 4, 85748 Garching, Germany
*Correspondence: stephan.sieber@mytum.de
http://dx.doi.org/10.1016/j.chembiol.2015.01.004

## SUMMARY

**The proteasome is responsible for the majority of protein degradation within eukaryotic cells and proteasome inhibitors have gained blockbuster status as anticancer drugs. Here, we introduce an analytical platform comprising reverse phase chromatography, intact protein mass spectrometry, and customized data analysis that allows a streamlined investigation of proteasome integrity and posttranslational modifications. We report the complete mass spectrometric assignment of all subunits of the yeast core particle, as well as of the human constitutive 20S proteasome and the human immunoproteasome, including phosphorylated isoforms of α7. Importantly, we found several batches of commercially available immunoproteasome to also contain constitutive catalytic subunits. Moreover, we applied the method to study the binding mechanisms of proteasome inhibitors, both validating the approach and providing a direct readout of subunit preferences complementary to biochemical methods. Collectively, our platform facilitates an easy, reliable and comprehensive detection of different types of covalent modifications on multisubunit protein complexes with high accuracy.**

The controlled degradation of proteins is of pivotal importance for cellular proteostasis. In eukaryotic cells, the proteasome is responsible for the majority of protein breakdown in both cytosol and nucleus (Hershko and Ciechanover, 1998; Kisselev and Goldberg, 2001; Voges et al., 1999). The 20S proteasomal core particle (CP) is composed of four seven-membered rings that are stacked corresponding to an α7:β7:β7:α7 stoichiometry (Figure 1A) (Groll et al., 1997; Lowe et al., 1995). Among all subunits, only β1c, β2c, and β5c are catalytically active. During an inflammatory state, they can be exchanged with alternative β1i, β2i, and β5i subunits to form the immunoproteasome (Huber et al., 2012; Unno et al., 2002). Every single catalytic subunit has its distinct cleavage site preference (Nussbaum et al., 1998) but they all share the general architecture as threonine protease, which gives rise to a number of intricate inhibition mechanisms by covalent inhibitors (Dubiella et al., 2014; Groll et al., 2000). Both the constitutive proteasome (cCP) as well as the immunoproteasome (iCP) are attractive drug targets for the treatment of cancer and autoimmune diseases, respectively.

Serine/threonine phosphorylation, N-terminal truncation, and N-terminal acetylation are the most common posttranslational modifications of the 20S proteasome (Lu et al., 2008; Uttenweiler-Joseph et al., 2008). Sample heterogeneity has become apparent from 2D gel electrophoresis due to multiple isoforms and has been analyzed via proteolytic digests with peptide-based mass spectrometry (Huang and Burlingame, 2005). While routinely feasible, this approach is characterized by several working steps and incomplete sequence coverage (Claverol et al., 2002; Wang et al., 2007). Intact protein mass spectrometry (IPMS) has been applied to proteasomes that have identical α and β subunits (Loo et al., 2005; Sharon et al., 2007). Approaches to study eukaryotic proteasomes by IPMS have been complicated by sample complexity and have thus been hampered by incomplete coverage as well as limited applicability (Dechavanne et al., 2013; Groll et al., 1999; Russell et al., 2013). MALDI-TOF analysis after 2D gel separation allowed the identification of all subunits (Uttenweiler-Joseph et al., 2008), however some isoforms could not be resolved (Bousquet-Dubouch et al., 2011). Most recently, a top-down analysis (Loo et al., 1990) with several fragmentation methods on a high-end Fourier transform-ion cyclotron resonance (FT-ICR) spectrometer allowed the investigation of cCP and its modifications after reverse phase separation (Lakshmanan et al., 2014). In this approach, spectra had to be selected manually for processing and a simulated gel view was used for plotting the results. This procedure illustrates a common challenge with complex samples for IPMS, since these samples typically consist of more species than there are peaks in the total ion current chromatogram. This not only makes the detection of all species by manual selection of spectra challenging but also prevents a robust and comprehensive assessment of sample properties. Here, we introduce an easy to implement and broadly applicable platform with automated software that enables comprehensive IPMS analysis of proteasome integrity, function, and inhibition.

We first validated the sample complexity by obtaining high-resolution mass spectra from online desalted yeast 20S proteasome (yCP) on an FT-ICR spectrometer. As anticipated, the deconvoluted data were of poor quality due to large spectral crowding. We then used an optimized gradient for C4-based reverse phase chromatography that enabled subunit separation (Figure 1B). Taking inspiration from the literature (Durbin et al., 2010; Lee et al., 2002; Tran et al., 2011), we devised software

 

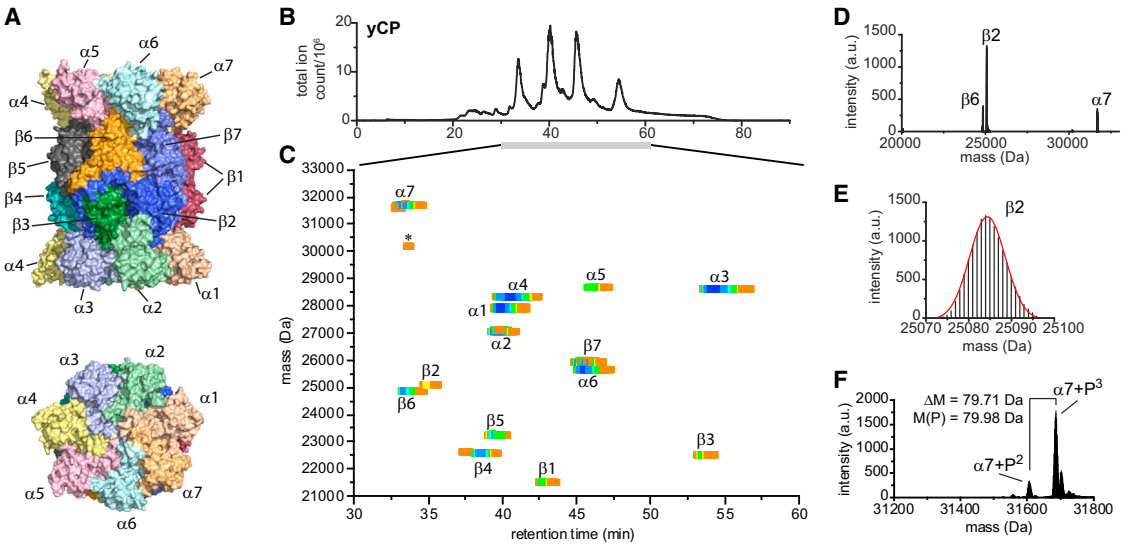


**Figure 1. Analysis of Yeast Proteasome**

(A) Surface representation of the yCP crystal structure (PDB ID 1RYP) in side and top view.

(B) Total ion count chromatogram of yCP separation.

(C) Map derived from rolling-window spectral deconvolution data analysis and subunit assignment. Colors depict arbitrary intensities obtained from deconvolution (blue/green/yellow/orange/red, from high to low intensity). The mass of the cluster denoted with an asterisk (*) corresponds to the mass of a C terminally truncated isoform of α7 (residues 2-273 with acylation and triple phosphorylation; expected mass: 30,191.4 Da; mass found: 30,190.5 Da).

(D) Deconvoluted spectrum showing the presence of subunit β2 (retention time window, 34.5–35.9 min).

(E) Mass determination of β2 through Gauss fitting ($M_{expected}$ = 25,085.44 Da, $M_{found}$ = 25,085.26 Da).

(F) Deconvoluted spectrum showing the 2-fold and 3-fold phosphorylated isoforms of subunit α7 (retention time window, 32.8–34.5 min). See also Figure S1 and Table S1.

for a rolling-window spectral deconvolution analysis (RoWinPro). In this automated analysis, sequential sets of scans (windows) covering the entire run are averaged and deconvoluted individually. RoWinPro is able to handle multiple jobs, e.g. for the analysis of several data sets or of one data set with different parameters. Its main advantage over other existing tools is its ability to process sequential windows within one data file, thus covering the entire chromatogram automatically. For the underlying deconvolution step, RoWinPro utilizes the Znova algorithm as implemented in the commercially available software Promass

**Table 1. Mass Spectrometric Assignment of the Yeast Proteasome Subunits**

| Subunit | Gene Name | Uniprot ID | Sequence[a] | Ac[b] | Expected Mass (Da) | Mass Found with Xtract (Da) | Δ (Da) | Mass Found with Znova (Da) |
|---|---|---|---|---|---|---|---|---|
| α1 | *PRS2* | P21243 | 2–252 | + | 27,911.65 | 27,911.28 | 0.4 | 27,911.7 |
| α2 | *PRE8* | P23639 | 2–250 | + | 27,072.66 | 27,072.60 | 0.1 | 27,071.7 |
| α3 | *PRE9* | P23638 | 2–258 | + | 28,625.04 | 28,624.22 | 0.8 | 28,624.5 |
| α4 | *PRE6* | P40303 | 2–254 | + | 28,349.89 | 28,349.12 | 0.8 | 28,350.1 |
| α5 | *PUP2* | P32379 | 1–260 | + | 28,659.11 | 28,658.04 | 1.1 | 28,658.5 |
| α6 | *PRE5* | P40302 | 1–234 | + | 25,646.01 | 25,645.87 | 0.1 | 25,645.4 |
| α7 | *PRE10* | P21242 | 2–288 | + | 31,686.90[c] | 31,686.15 | 0.7 | 31,686.3 |
| β1 | *PRE3* | P38624 | 20–215 | – | 21,494.18 | 21,493.79 | 0.4 | 21,493.9 |
| β2 | *PUP1* | P25043 | 30–261 | – | 25,085.44 | 25,085.26 | 0.2 | 25,084.4 |
| β3 | *PUP3* | P25451 | 2–205 | + | 22,515.68 | 22,515.16 | 0.5 | 22,514.9 |
| β4 | *PRE1* | P22141 | 1–198 | + | 22,558.68 | 22,558.33 | 0.4 | 22,557.7 |
| β5 | *PRE2* | P30656 | 76–287 | – | 23,300.25 | 23,299.86 | 0.4 | 23,299.4 |
| β6 | *PRE7* | P23724 | 20–241 | – | 24,850.88 | 24,850.75 | 0.1 | 24,850.1 |
| β7 | *PRE4* | P30657 | 34–266 | – | 25,919.51 | 25,920.19 | –0.7 | 25,919.6 |

[a]Sequence denotes the first and last amino acid in the processed protein.

[b]Ac denotes whether the subunit is acylated (+) or not (–). The N-termini of β1, β2, β5, β6, and β7 are protected against N-terminal acetylation by propeptides that are cleaved off autoprocessively during assembly of the proteasome (Groll et al., 1999).

[c]The major species of α7 was found to be three-times phosphorylated.

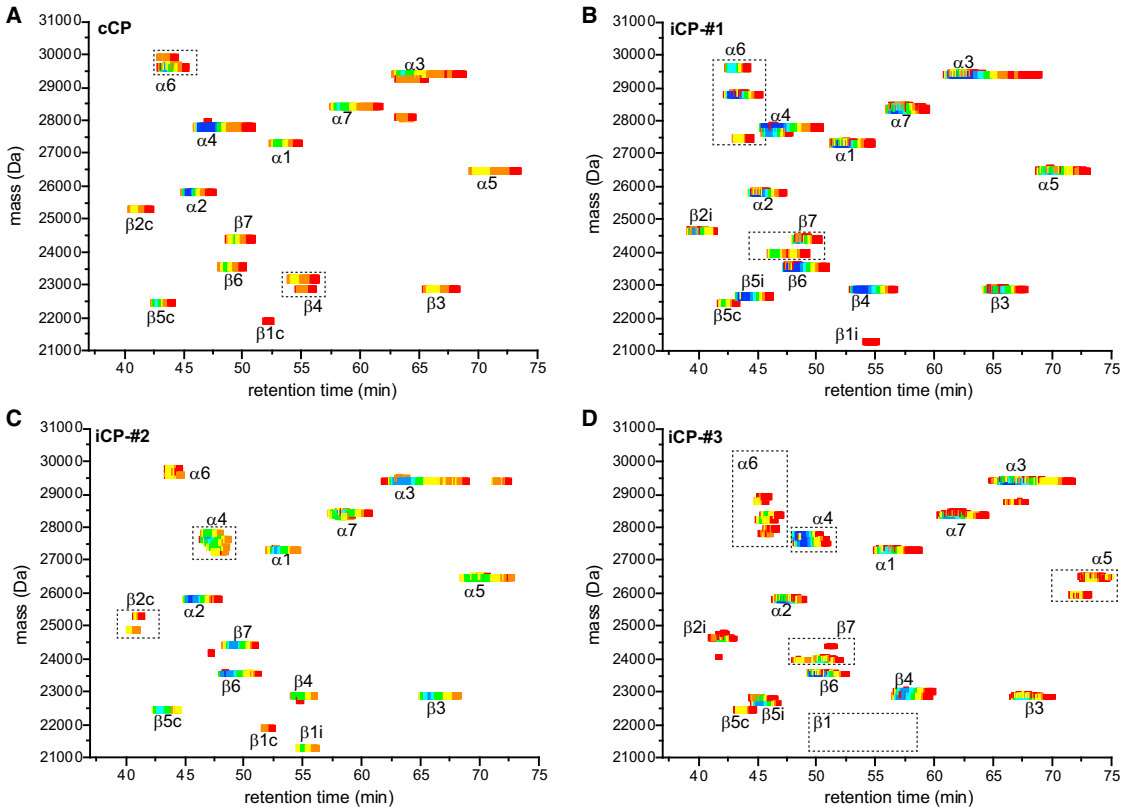


**Figure 2. Maps Derived from Rolling-Window Spectral Deconvolution Data Analysis**

(A–D) Human constitutive proteasome (cCP, A), immunoproteasome (iCP) sample 1 (B), sample 2 (C), and sample 3 (D).

Selected partially degraded/alternatively processed or missing subunits are highlighted with dashed boxes. See also Figure S2, Figure S3, and Table S2.

(Zhang and Marshall, 1998). However, any deconvolution program that features a command-line-based interface can be implemented. In order to visualize the results, a sample map can be constructed by plotting detected protein masses over the mean retention times of the analyzed scans. We then subjected these data to intensity-weighted *k*-means clustering. Clusters on the yCP sample map could be assigned to all 14 subunits of the proteasome with distinct posttranslational modifications (phosphorylation, truncation, and acetylation), in agreement with annotations in the Uniprot database (Figure 1C; Table 1). We then selected spectra with maximal intensity for each subunit and performed high accuracy mass determination using deconvolution with the Xtract algorithm and Gauss fitting (Figure S1). Such analysis enabled us to obtain high-quality spectra in isotopic resolution of the β2 subunit that had so far been elusive to mass spectrometry (Groll et al., 1999) (Figures 1D and 1E). While no intensity was observed for the mass anticipated for subunit α7, we obtained two clusters that were heavier by +160 Da and +240 Da and were thus assigned to 2-fold and 3-fold phosphorylated isoforms, respectively (Figure 1F). For all other subunits, no such clusters corresponding to phosphorylated isoforms were found. We determined the stoichiometry of these isoforms through deconvolution with four different algorithms, which gave similar results. 82.5% ± 2.2% (mean ± SD) of the α7 signal was derived from the 3-fold phosphorylated isoform while correspondingly 17.5% ± 2.2% was derived from the 2-fold phosphorylated isoform (Table S1). α7 phosphorylation at Ser258, Ser263, and Ser264 was previously identified by proteomic experiments (Soufi et al., 2009). Here, we report that α7 phosphorylation is the only major phosphorylation observed in yCP. Our data on the protein level thus complement proteomic data with the quantitative phosphorylation stoichiometry, which can be difficult to obtain through peptide-based methods (Carpy et al., 2014).

Next, we turned to the human constitutive proteasome and to the human immunoproteasome and subjected them to a similar analysis (Figure 2; Figure S2). Our analytical platform allowed for the complete assignment of all subunits with mass accuracies <1 Da (Table 2; Figure S2). Monophosphorylation represented the dominant modification of α7 while all other subunits were only detected as unphosphorylated isoforms. This finding is in agreement with previous results (Lakshmanan et al., 2014; Olsen et al., 2010; Zong et al., 2008). The degree of α7 monophosphorylation was determined highly reproducibly and robustly from ten independent samples and three different cCP batches to be 95.7% ± 1.1% (mean ± SD, Table S2). α7 phosphorylation has been implicated with an increased 20S-19S interaction (Bose et al., 2004). While the maps of the cCP samples were generally of high quality (Figure 2A), the data derived from three different batches of commercially obtained iCP showed a higher degree of heterogeneity. Importantly, all three iCP samples contained substantial amounts of the respective constitutive subunits, partly as the only detectable catalytic species (as for β2c and

**Table 2. Mass Spectrometric Assignment of the Human Constitutive Proteasome and the Human Immunoproteasome Subunits**

| Subunit | Gene Name | Uniprot ID | Sequence | Ac | Expected Mass (Da) | Mass Found with Xtract (Da) | Δ (Da) | Mass Found with Znova (Da) |
|---|---|---|---|---|---|---|---|---|
| α1 | *PSMA6* | P60900 | 2–246 | + | 27,310.27 | 27,309.60 | 0.7 | 27,309.6 |
| α2 | *PSMA2* | P25787 | 2–234 | + | 25,809.38 | 25,809.14 | 0.3 | 25,808.8 |
| α3 | *PSMA4* | P25789 | 2–261 | + | 29,394.61 | 29,394.28 | 0.4 | 29,393.9 |
| α4 | *PSMA7* | O14818 | 2–248 | + | 27,797.64 | 27,797.69 | 0.0 | 27,797.5 |
| α5 | *PSMA5* | P28066 | 1–241 | + | 26,453.04 | 26,452.53 | 0.5 | 26,452.9 |
| α6 | *PSMA1* | P25786 | 1–263 | + | 29,597.60 | 29,597.07 | 0.6 | 29,596.7 |
| α7 | *PSMA3* | P25788 | 2–255 | + | 28,424.04[a] | 28,423.57 | 0.5 | 28,423.8 |
| β1c | *PSMB6* | P28072 | 35–239 | – | 21,903.87 | 21,903.29 | 0.6 | 21,903.2 |
| β2c | *PSMB7* | Q99436 | 44–277 | – | 25,294.97 | 25,294.44 | 0.6 | 25,294.3 |
| β3 | *PSMB3* | P49720 | 2–205 | + | 22,859.74 | 22,859.47 | 0.3 | 22,859.7 |
| β4 | *PSMB2* | P49721 | 1–201 | + | 22,878.28 | 22,877.76 | 0.6 | 22,878.2 |
| β5c | *PSMB5* | P28074 | 60–263 | – | 22,458.34 | 22,457.87 | 0.5 | 22,457.8 |
| β6 | *PSMB1* | P20618 | 29–241 | – | 23,548.94 | 23,548.32 | 0.7 | 23,547.9 |
| β7 | *PSMB4* | P28070 | 46–264 | – | 24,391.75 | 24,391.21 | 0.6 | 24,391.5 |
| β1i | *PSMB9* | P28065 | 21–219 | – | 21,276.02 | 21,275.45 | 0.6 | 21,275.2 |
| β2i | *PSMB10* | P40306 | 40–273 | – | 24,648.25[b] | 24,630.75/24,647.47 | 0.8 | 24,630.3/24,647.5 |
| β5i | *PSMB8* | P28062 | 73–276 | – | 22,659.60 | 22,659.61 | 0.0 | 22,659.4 |

Subunits are numbered according to their homology to the respective yeast counterparts. Of note, different numbering schemes are present in the literature (Dechavanne et al., 2013). Localization of cCP subunit modifications through top-down analysis has been reported recently by Lakshmanan et al. (2014).

[a] α7 was found to be monophosphorylated.

[b] The majority of β2i appeared as a lighter isoform (−17 Da) in all samples; only a weak signal for the canonical β2i was detected.

β5c in iCP sample 2, Figure 2C) while in sample 3 (Figure 2D) the catalytic β1i subunit was apparently missing. Whereas mouse immunoproteasome can be purified from mouse liver after iCP enrichment through viral infection, human iCP is typically purified from cells that express both the constitutive and immunoproteasome-specific subunits, likely explaining these results. In addition, the existence of intermediary-type proteasomes with a mixed composition of catalytic subunits has been reported (Bousquet-Dubouch et al., 2011). We detected additional clusters shifted to lower masses with regard to the parent noncatalytic subunits which were assigned to N-terminal truncation products (marked in dashed boxes). In some cases, the full-length isoform was completely missing (as α6 in sample 3, Figure 2D) or had become a minor species (as α4 in sample 2, Figure 2C). Unexpectedly, the β2i subunit appeared as an isoform in all samples as the major species that was ~17 Da lighter than the canonical sequence would suggest. This mass difference would be consistent with an Asn → Pro or with a Met → Asn mutation (more complicated patterns of mutations are possible as well; however, the precise determination of the mass difference is precluded by the presence of multiple oxidized species). Of note, variants corresponding to point mutations as a result of SNPs have been described for other subunits (Uttenweiler-Joseph et al., 2008). While our analysis cannot match the localization precision of peptide-based methods, it provides insights into sample integrity that are difficult to obtain from conventional proteomic approaches. All observed alterations might have important consequences for structural integrity and catalytic activity of the proteasome. Mass spectrometry (MS)-based subunit mapping can assess this heterogeneity (Claverol et al., 2002) and variance in different samples beyond the capabilities of 2D gel electrophoresis, and we believe this heterogeneity has to be considered when discussing results derived from such immunoproteasome batches. We also established the analysis on a common low-resolution ion-trap mass spectrometer (Figure S3), ensuring a broad applicability of the method.

Clinically applied proteasome inhibitors such as bortezomib (Velcade) and carfilzomib (Kyprolis) have gained blockbuster status as anticancer drugs (Huber et al., 2012; Kisselev and Goldberg, 2001). Moreover, immunoproteasome-specific inhibitors are currently being developed by both industrial and academic groups with promising results against diseases characterized by aberrant immune function (Basler et al., 2014). Different statements have been made in the literature regarding the combination of subunits that needs to be inactivated to evoke cytotoxicity, although β5c/β5i are generally assumed to be the most important targets. Several techniques exist to assess subunit specificity of proteasome inhibitors. Fluorogenic substrates are widely used, however, results are at times questioned because of cross-reactivity with other proteases or similar substrate preferences (e.g. β5c and β1i). Moreover, subunit-specific activity-based probes exist (Li et al., 2014); however, their readout by gel fluorescence imaging restricts its use for the analysis of catalytic subunits and does not inform about inhibition mechanisms. Crystallography was recently applied for this purpose (Stein et al., 2014) but, despite the detailed insights, its low throughput and restriction to well-crystallizable forms of the proteasome limit its application (Dubiella et al., 2014).

We reasoned that our approach might be complementing these techniques for covalent inhibitors and we consequently

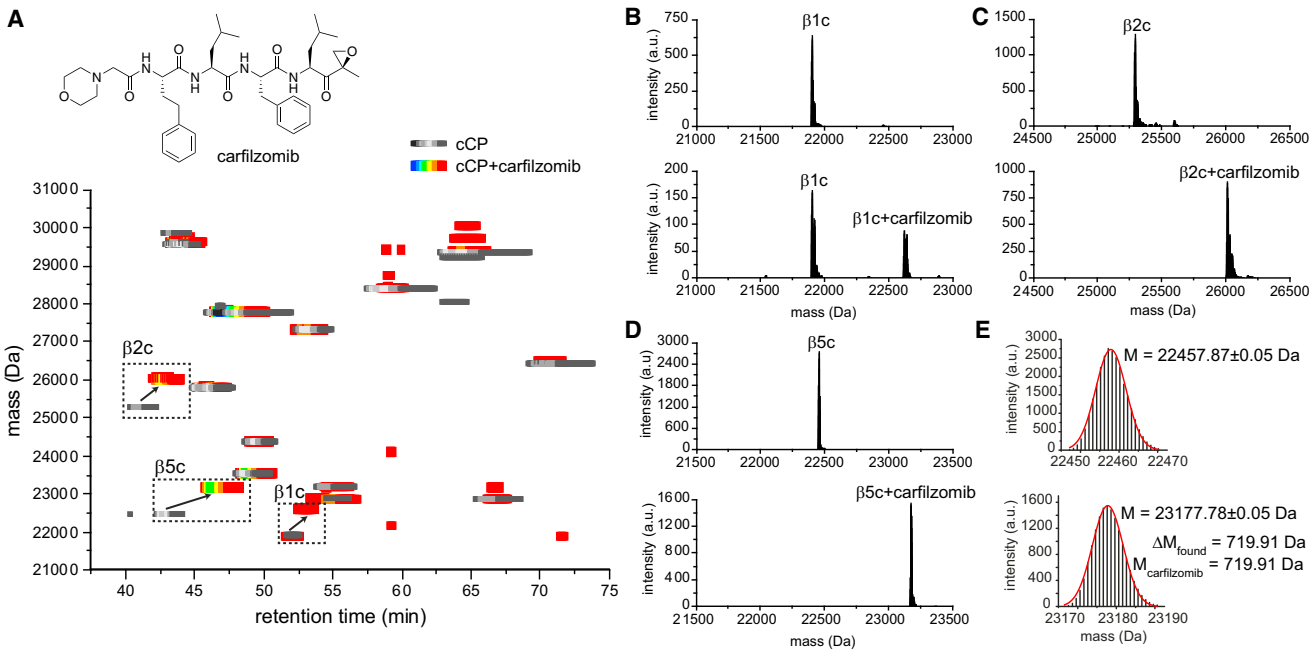


**Figure 3. Analysis of Human cCP Treated with 25 μM Carfilzomib**

(A–D) (A) Structure of carfilzomib and overlay of maps from untreated cCP (gray) and carfilzomib-treated cCP (color). Shifts of the catalytic subunits are indicated in boxes. Deconvoluted spectra showing the β1c (B), β2c (C), and β5c (D) subunits (upper panels, untreated cCP; lower panels, treated cCP).

(E) Gauss-fitting analysis of β5c spectral data confirming the mass of the carfilzomib adduct.

See also Figure S4.

applied our analytical platform to the investigation of subunit specificity and inhibitor mechanisms. First, we analyzed the effects of the well-characterized, irreversibly binding inhibitor carfilzomib on the catalytic subunits of cCP (Harshbarger et al., 2015; Huber et al., 2015) (Figure 3A). Overlay of the deconvolution maps clearly showed the disappearance of the clusters representing unmodified β2c and β5c subunits while nearby new clusters appeared; other subunits remained unchanged. We then selected spectra for Xtract deconvolution and found that these new clusters correspond to masses of β2c:carfilzomib and β5c:carfilzomib adducts (Figures 3B–3E). A minor cluster with a β1c:carfilzomib adduct was identified, which is in agreement with incomplete binding as evident from the deconvolution spectra (Figure 3B). When treated with a lower concentration (2.5 μM, see Figure S4B), modification of only β5c was observed, which is in line with the published β5c selectivity. Furthermore, we analyzed samples of cCP incubated with MG-132 and a vinyl sulfone-based inhibitor (Figures S4C–S4E), all consistently showing β5c-modified species. Notably, due to the protein concentration in the sample (0.5 mg/ml, corresponding to 1.4 μM per catalytic subunit), this analysis cannot be used to infer compound potencies as these are usually in the nanomolar range. However, a competition experiment with several covalent inhibitors present in the reaction can be used for a relative comparison of compound potencies.

Collectively, the platform reported herein facilitates a fast, reliable, and comprehensive evaluation of different proteasome samples (Figure 4). We have recently applied this method to the study of short-lived species and novel chemical modifications, demonstrating its capacity to contribute to the investigation of inhibitor binding mechanisms (Dubiella et al., 2014). Moreover, it opens the possibility of screening for covalent binders of noncatalytic subunits. Its capabilities greatly surpass 2D gel electrophoresis and we therefore expect it to be useful for quality control and sample characterization purposes. In addition, the platform can be used to compare proteasome samples derived from cells with different genomic backgrounds in order to assist in the investigation of proteasome assembly, subunit processing, and regulation through posttranslational modifications. Compiled versions and documentation of the rolling-window deconvolution analysis program are available for download at http://www.oc2.ch.tum.de free of charge.

## SIGNIFICANCE

**IPMS is a powerful tool that can inform about protein complex integrity and the stoichiometry of posttranslational modification, two properties that are difficult to obtain through peptide-based mass spectrometric methods. However, there are typically more species than peaks in the total ion current chromatogram in complex samples, which makes the detection of all species by manual selection of spectra challenging. Here, we introduce a program that facilitates an automated, comprehensive data analysis, and creates data for an intuitive visualization of the results in the form of a sample map. We apply this analysis technique to the investigation of several proteasome samples, validating the approach, proving its complementarity to existing methods, and showing its usefulness in protein biochemistry and chemical biology research.**

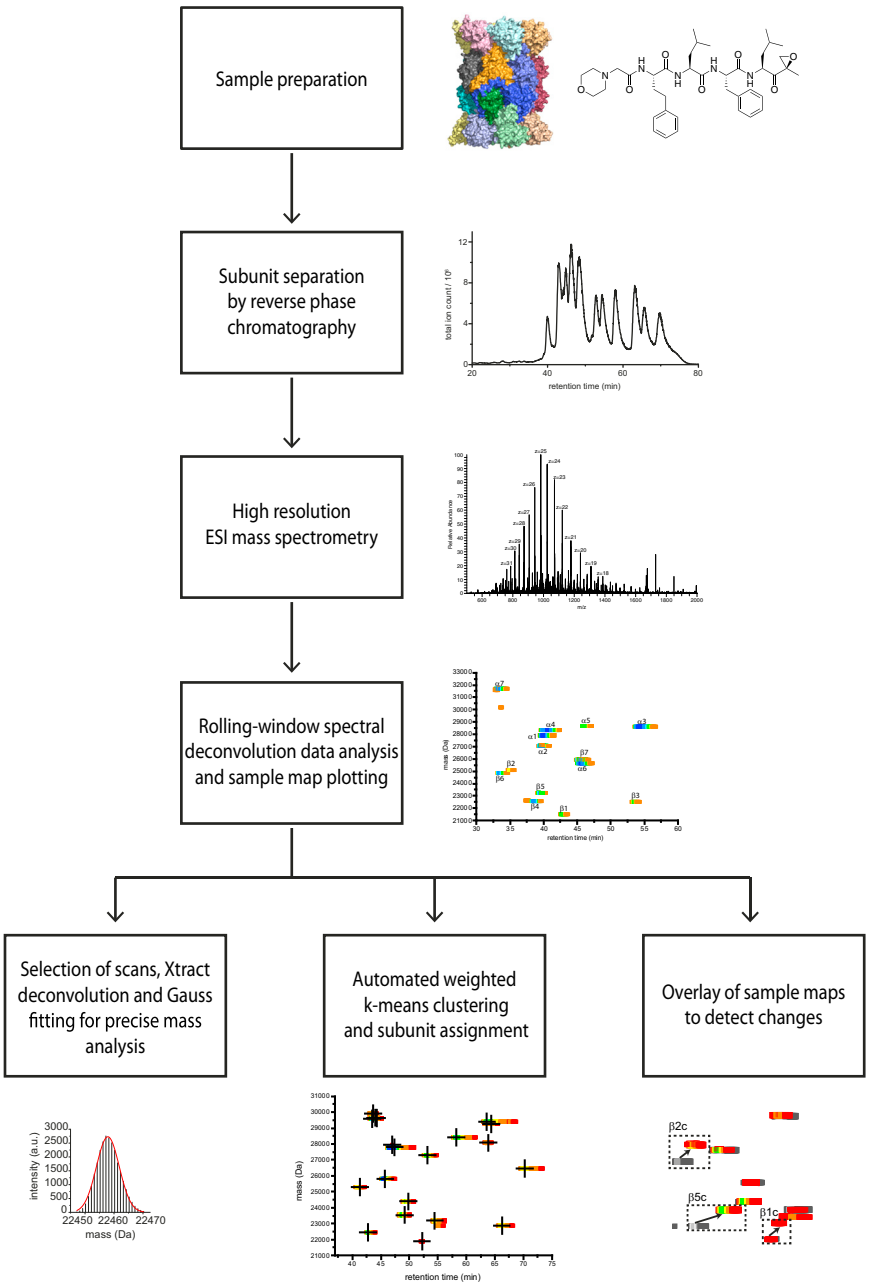


**Figure 4. Schematic Depiction of the Workflow.**

## EXPERIMENTAL PROCEDURES

### Sample Preparation

Yeast proteasome was freshly purified from *Saccharomyces cerevisiae* as described previously (Groll et al., 2006). Human constitutive proteasome and human immunoproteasome were obtained from Boston Biochem. Inhibitors were either purchased from Selleckchem or synthesized as described previously (Stein et al., 2014). Proteasome solution (0.5 mg/ml) in 50 mM HEPES (pH 7.6), 100 mM NaCl, 1 mM DTT (for cCP and iCP) in 20 mM MES (pH 6.8), 150 mM NaCl (for yCP) was incubated with indicated inhibitor concentrations for 12 hr at room temperature and then brought to 30% (v/v) acetonitrile.

### Reverse Phase Chromatography and IPMS

Analyses were carried out on a Dionex UltiMate 3000 high-performance liquid chromatography (HPLC) system coupled to a Thermo Scientific LTQ-FT Ultra mass spectrometer with an electrospray ionization (ESI) source (room temperature; ionization voltage, 3.9 kV; tube lens, 110 V; capillary voltage, 20 V; sheath gas, auxiliary gas, and sweep gas, off). A heated ESI source could also be used (vaporizer temperature, 70°C; ionization voltage, 4.45 kV; tube lens, 120 V; capillary voltage, 30 V; sheath gas, 30 arb; auxiliary gas, 10 arb; sweep gas, off), demonstrating the broad applicability and transferability of the method. Eluent A consisted of water with 0.1% formic acid, eluent B consisted either of 90% acetonitrile and 10% water with 0.1% formic acid or 100% acetonitrile with 0.1% formic acid. All solvents were of liquid chromatography LC/MS grade (Sigma-Aldrich). Samples (10 µl, corresponding to 4.7 pmol/3.5 µg of proteasome per run) were separated on a C4 column (BioBasic-4, Thermo Scientific, 150 mm × 1 mm, 5 µm; flow, 0.050 ml/min) with a gradient from 30% to 60% B over 60 min preceded by a 15 min equilibration step at 30% B and followed by a washing step at 100% B for 5 min. The mass spectrometer was run in positive mode, collecting full scans at high resolution ($R$ = 200,000) from $m/z$ 500 to $m/z$ 2,000. For the low-resolution experiment, the sample was analyzed on a Dionex UltiMate 3000 HPLC system coupled to a Thermo Scientific LCQ Fleet mass spectrometer with a heated ESI source (source temperature, 39°C; ionization voltage, 4.45 kV; tube lens, 90 V; capillary voltage, 31 V; sheath gas, 30 arb; auxiliary gas, 10 arb; sweep gas, off). Eluent A consisted of water with 0.1% formic acid, eluent B consisted of 100% acetonitrile with 0.1% formic acid. All solvents were of LC/MS grade (Sigma-Aldrich). The sample was separated on a C4 column (BioBasic-4, Thermo Scientific, 150 mm × 1 mm, 5 µm; flow, 0.050 ml/min) with a gradient from 30% to 60% B over 60 min proceeded by a 15 min equilibration step at 30% B and followed by a washing step at 100% B for 5 min. The mass spectrometer was run in positive mode collecting ion-trap scans at scan rate "normal" from $m/z$ 300 to $m/z$ 2,000.

### Data Analysis

Xcalibur raw files were processed using customized software (RoWinPro, available for download at http://www.oc2.ch.tum.de) with rolling-window deconvolution analysis. The software uses the Xcalibur developer kit (XDK) to retrieve and average scans (window size, 10 scans for high-resolution data, 40 scans for low-resolution data; parameters can be specified in a graphical user interface) and analyzes them with the Znova deconvolution algorithm as implemented in the commercially available software Promass from Novatia, LLC (Zhang and Marshall, 1998) (input, 600–1,600 $m/z$; output, 18,000–36,000 Da; 1 Da mass step size; peak width, 3; merge width, 0.3; minimum score, 2; S/N threshold, 2; smooth width, 7; number of smooths, 2). Output files contain a list of detected species (retention time in minutes, mass in Daltons, intensity in arbitrary units) and were plotted with Microcal OriginPro 9.1 with a cut-off at 80% of the summed intensity (usually corresponding to the top 10%–50% of all data points) to reduce noise. The color scale was set to arbitrary values in order to fully cover the intensity range of the analyzed sample. Spectra containing subunits of interest were subsequently averaged with Xcalibur and analyzed

by Thermo Scientific Xtract (Senko et al., 1995) for deconvolution and quantification. Gauss fits of deconvoluted Xtract spectra were carried out with Microcal OriginPro. MagTran (Zhang and Marshall, 1998) and Mann's Algorithm (Mann et al., 1989) (as implemented in MagTran) were used to confirm deconvolution results. Intensity-weighted *k*-means clustering (initial clusters, 20) was carried out with OriginPro and MATLAB. Cluster centers were plotted as crosses. See Figure 4 for a visual depiction of the workflow and the User Guide available online for further details on the analysis software.

## SUPPLEMENTAL INFORMATION

Supplemental Information includes two tables, four figures, the RoWinPro User Guide, and the associated software and can be found with this article online at http://dx.doi.org/10.1016/j.chembiol.2015.01.004.

## AUTHOR CONTRIBUTIONS

M.G. and M.H. performed measurements and analyzed data. C.D. prepared samples. A.D. and M.G. wrote the analysis software. M.Gr. and S.A.S. supervised the project. M.G. wrote the paper with input from all authors.

## ACKNOWLEDGMENTS

We thank Nina Bach, Katja Bäuml, Burghard Cordes, Richard Feicht, and Max Koch for technical assistance. We gratefully acknowledge funding from the Deutsche Forschungsgemeinschaft through SFB1035, SFB749, FOR1406, CIPS$^{M}$, and from the European Research Council.

Received: November 11, 2014
Revised: December 22, 2014
Accepted: January 13, 2015
Published: February 26, 2015

## REFERENCES

Basler, M., Mundt, S., Muchamuel, T., Moll, C., Jiang, J., Groettrup, M., and Kirk, C.J. (2014). Inhibition of the immunoproteasome ameliorates experimental autoimmune encephalomyelitis. EMBO Mol. Med. *6*, 226–238.

Bose, S., Stratford, F.L., Broadfoot, K.I., Mason, G.G., and Rivett, A.J. (2004). Phosphorylation of 20S proteasome alpha subunit C8 (alpha7) stabilizes the 26S proteasome and plays a role in the regulation of proteasome complexes by gamma-interferon. Biochem. J. *378*, 177–184.

Bousquet-Dubouch, M.P., Fabre, B., Monsarrat, B., and Burlet-Schiltz, O. (2011). Proteomics to study the diversity and dynamics of proteasome complexes: from fundamentals to the clinic. Expert Rev. Proteomics *8*, 459–481.

Carpy, A., Krug, K., Graf, S., Koch, A., Popic, S., Hauf, S., and Macek, B. (2014). Absolute proteome and phosphoproteome dynamics during the cell cycle of *Schizosaccharomyces pombe* (Fission Yeast). Mol. Cell. Proteomics *13*, 1925–1936.

Claverol, S., Burlet-Schiltz, O., Girbal-Neuhauser, E., Gairin, J.E., and Monsarrat, B. (2002). Mapping and structural dissection of human 20 S proteasome using proteomic approaches. Mol. Cell. Proteomics *1*, 567–578.

Dechavanne, V., Vilbois, F., Glez, L., and Antonsson, B. (2013). Purification and separation of the 20S immunoproteasome from the constitutive proteasome and identification of the subunits by LC-MS. Protein Expression Purif. *87*, 100–110.

Dubiella, C., Cui, H., Gersch, M., Brouwer, A.J., Sieber, S.A., Kruger, A., Liskamp, R.M., and Groll, M. (2014). Selective immunoproteasome inhibition by ligand-induced active site crosslinking. Angew. Chem. Int. Ed. Engl. *53*, 11969–11973.

Durbin, K.R., Tran, J.C., Zamdborg, L., Sweet, S.M., Catherman, A.D., Lee, J.E., Li, M., Kellie, J.F., and Kelleher, N.L. (2010). Intact mass detection, interpretation, and visualization to automate Top-Down proteomics on a large scale. Proteomics *10*, 3589–3597.

Groll, M., Ditzel, L., Lowe, J., Stock, D., Bochtler, M., Bartunik, H.D., and Huber, R. (1997). Structure of 20S proteasome from yeast at 2.4 A resolution. Nature *386*, 463–471.

Groll, M., Heinemeyer, W., Jager, S., Ullrich, T., Bochtler, M., Wolf, D.H., and Huber, R. (1999). The catalytic sites of 20S proteasomes and their role in subunit maturation: a mutational and crystallographic study. Proc. Natl. Acad. Sci. USA *96*, 10976–10983.

Groll, M., Kim, B., Kairies, N., Huber, R., and Crews, C.M. (2000). Crystal structure of epoxomicin:20S proteasome reveals a molecular basis for selectivity of $\alpha',\beta'$-epoxyketone proteasome inhibitors. J. Am. Chem. Soc. *122*, 1237–1238.

Groll, M., Huber, R., and Potts, B.C. (2006). Crystal structures of Salinosporamide A (NPI-0052) and B (NPI-0047) in complex with the 20S proteasome reveal important consequences of beta-lactone ring opening and a mechanism for irreversible binding. J. Am. Chem. Soc. *128*, 5136–5141.

Harshbarger, W., Miller, C., Diedrich, C., and Sacchettini, J. (2015). Crystal structure of the human 20S proteasome in complex with carfilzomib. Structure *23*, 418–424.

Hershko, A., and Ciechanover, A. (1998). The ubiquitin system. Annu. Rev. Biochem. *67*, 425–479.

Huang, L., and Burlingame, A.L. (2005). Comprehensive mass spectrometric analysis of the 20S proteasome complex. Methods Enzymol. *405*, 187–236.

Huber, E.M., Basler, M., Schwab, R., Heinemeyer, W., Kirk, C.J., Groettrup, M., and Groll, M. (2012). Immuno- and constitutive proteasome crystal structures reveal differences in substrate and inhibitor specificity. Cell *148*, 727–738.

Huber, E.M., Heinemeyer, W., and Groll, M. (2015). Bortezomib-resistant mutant proteasomes: structural and biochemical evaluation with carfilzomib and ONX 0914. Structure *23*, 407–417.

Kisselev, A.F., and Goldberg, A.L. (2001). Proteasome inhibitors: from research tools to drug candidates. Chem. Biol. *8*, 739–758.

Lakshmanan, R., Wolff, J.J., Alvarado, R., and Loo, J.A. (2014). Top-down protein identification of proteasome proteins with nanoLC-FT-ICR-MS employing data-independent fragmentation methods. Proteomics *14*, 1271–1282.

Lee, S.W., Berger, S.J., Martinovic, S., Pasa-Tolic, L., Anderson, G.A., Shen, Y., Zhao, R., and Smith, R.D. (2002). Direct mass spectrometric analysis of intact proteins of the yeast large ribosomal subunit using capillary LC/FTICR. Proc. Natl. Acad. Sci. USA *99*, 5942–5947.

Li, H., van der Linden, W.A., Verdoes, M., Florea, B.I., McAllister, F.E., Govindaswamy, K., Elias, J.E., Bhanot, P., Overkleeft, H.S., and Bogyo, M. (2014). Assessing subunit dependency of the *Plasmodium* proteasome using small molecule inhibitors and active site probes. ACS Chem. Biol. *9*, 1869–1876.

Loo, J.A., Edmonds, C.G., and Smith, R.D. (1990). Primary sequence information from intact proteins by electrospray ionization tandem mass spectrometry. Science *248*, 201–204.

Loo, J.A., Berhane, B., Kaddis, C.S., Wooding, K.M., Xie, Y., Kaufman, S.L., and Chernushevich, I.V. (2005). Electrospray ionization mass spectrometry and ion mobility analysis of the 20S proteasome complex. J. Am. Soc. Mass Spectrom. *16*, 998–1008.

Lowe, J., Stock, D., Jap, B., Zwickl, P., Baumeister, W., and Huber, R. (1995). Crystal structure of the 20S proteasome from the archaeon *T. acidophilum* at 3.4 A resolution. Science *268*, 533–539.

Lu, H.J., Zong, C.G., Wang, Y.J., Young, G.W., Deng, N., Souda, P., Li, X.H., Whitelegge, J., Drews, O., Yang, P.Y., et al. (2008). Revealing the dynamics of the 20 S proteasome phosphoproteome. Mol. Cell. Proteomics *7*, 2073–2089.

Mann, M., Meng, C.K., and Fenn, J.B. (1989). Interpreting mass-spectra of multiply charged ions. Anal. Chem. *61*, 1702–1708.

Nussbaum, A.K., Dick, T.P., Keilholz, W., Schirle, M., Stevanovic, S., Dietz, K., Heinemeyer, W., Groll, M., Wolf, D.H., Huber, R., et al. (1998). Cleavage motifs of the yeast 20S proteasome beta subunits deduced from digests of enolase 1. Proc. Natl. Acad. Sci. USA *95*, 12504–12509.

Olsen, J.V., Vermeulen, M., Santamaria, A., Kumar, C., Miller, M.L., Jensen, L.J., Gnad, F., Cox, J., Jensen, T.S., Nigg, E.A., et al. (2010). Quantitative phosphoproteomics reveals widespread full phosphorylation site occupancy during mitosis. Sci. Signal. *3*, ra3.

 

Russell, J.D., Scalf, M., Book, A.J., Ladror, D.T., Vierstra, R.D., Smith, L.M., and Coon, J.J. (2013). Characterization and quantification of intact 26S proteasome proteins by real-time measurement of intrinsic fluorescence prior to top-down mass spectrometry. PLoS One *8*, e58157.

Senko, M.W., Beu, S.C., and McLafferty, F.W. (1995). Automated assignment of charge states from resolved isotopic peaks for multiply-charged ions. J. Am. Soc. Mass Spectr. *6*, 52–56.

Sharon, M., Witt, S., Glasmacher, E., Baumeister, W., and Robinson, C.V. (2007). Mass spectrometry reveals the missing links in the assembly pathway of the bacterial 20 S proteasome. J. Biol. Chem. *282*, 18448–18457.

Soufi, B., Kelstrup, C.D., Stoehr, G., Frohlich, F., Walther, T.C., and Olsen, J.V. (2009). Global analysis of the yeast osmotic stress response by quantitative proteomics. Mol. Biosyst. *5*, 1337–1346.

Stein, M.L., Cui, H., Beck, P., Dubiella, C., Voss, C., Kruger, A., Schmidt, B., and Groll, M. (2014). Systematic comparison of peptidic proteasome inhibitors highlights the alpha-ketoamide electrophile as an auspicious reversible lead motif. Angew. Chem. Int. Ed. Engl. *53*, 1679–1683.

Tran, J.C., Zamdborg, L., Ahlf, D.R., Lee, J.E., Catherman, A.D., Durbin, K.R., Tipton, J.D., Vellaichamy, A., Kellie, J.F., Li, M.X., et al. (2011). Mapping intact protein isoforms in discovery mode using top-down proteomics. Nature *480*, 254–258.

Unno, M., Mizushima, T., Morimoto, Y., Tomisugi, Y., Tanaka, K., Yasuoka, N., and Tsukihara, T. (2002). The structure of the mammalian 20S proteasome at 2.75 A resolution. Structure *10*, 609–618.

Uttenweiler-Joseph, S., Claverol, S., Sylvius, L., Bousquet-Dubouch, M.P., Burlet-Schiltz, O., and Monsarrat, B. (2008). Toward a full characterization of the human 20S proteasome subunits and their isoforms by a combination of proteomic approaches. Methods Mol. Biol. *484*, 111–130.

Voges, D., Zwickl, P., and Baumeister, W. (1999). The 26S proteasome: a molecular machine designed for controlled proteolysis. Annu. Rev. Biochem. *68*, 1015–1068.

Wang, X., Chen, C.F., Baker, P.R., Chen, P.L., Kaiser, P., and Huang, L. (2007). Mass spectrometric characterization of the affinity-purified human 26S proteasome complex. Biochemistry *46*, 3553–3565.

Zhang, Z., and Marshall, A.G. (1998). A universal algorithm for fast and automated charge state deconvolution of electrospray mass-to-charge ratio spectra. J. Am. Soc. Mass Spectrom. *9*, 225–233.

Zong, C., Young, G.W., Wang, Y., Lu, H., Deng, N., Drews, O., and Ping, P. (2008). Two-dimensional electrophoresis-based characterization of post-translational modifications of mammalian 20S proteasome complexes. Proteomics *8*, 5025–5037.